CrossMark

ORIGINAL PAPER

Optimized synthesis of hydroxypropyl cellulose-*g*-poly(ε-caprolactone) network

Marzieh Jahangiri[1] · Massoumeh Bagheri[1] · Fahimeh Farshi[1] ·
Farhang Abbasi[2]

Abstract The objective of this study was the synthesis of copolymer networks based on poly (ε-caprolactone) (PCL), hydroxypropyl cellulose (HPC) and hexamethylene diisocyanate (HDI) via bulk graft copolymerization followed by crosslinking (using routes I and II), and subsequent optimization of the process by response surface methodology (RSM). The studied reaction parameters were: (i) monomer content (weight ratio of CL/HPC), (ii) amount of catalyst, and (iii) amount of crosslinker. FT-IR and ^{1}H NMR results confirmed that the grafting of PCL onto HPC and subsequent crosslinking through terminal hydroxyl groups of PCL grafts by HDI were performed successfully. Through differential scanning calorimetry (DSC) and X-ray diffraction analysis (XRD), it was found that the crystallinity of grafted polymers depended on the amount of grafted PCL and degree of crosslinking. In modeling of the process using RSM, the coefficient of determination (R^2) for the models (97.3 and 93.3 % for two routes) as well as the probability ($p < 0.0001$) revealed high significance of the regression models. Also it was found that the obtained systems possessed T_ms between 42.94 and 54.57 °C (route I) and 32.49–46.30 °C (route II) that were tunable by the monomer content, catalyst and crosslinker amounts. RSM provided a useful tool to select in a fast way the proper experimental conditions to synthesize crosslinked HPC-*g*-PCL copolymer as a novel biocompatible and biodegradable shape memory polymer with adjustable switching temperature and potential biomedical applications, which would be further studied in the future.

Keywords Poly (ε-caprolactone) · Hydroxypropyl cellulose · Graft copolymer · Optimization · Response surface methodology

Introduction

Recently, chemical modification of biodegradable polymers has become an important method to generate valuable materials with improved properties and expand their applications especially in biomedical fields. Poly (ε-caprolactone) (PCL) as a semicrystalline biodegradable polymer, is one of the most important polymer with relatively low melting temperature and good mechanical properties. For biomedical applications, the biodegradability nature of the polymers and adjustment of their T_m around the human body temperature (37–39 °C) are the essential key factors and a challenging field for researchers [1, 2]. From this aspect, PCL is a good choice as a biocompatible and biodegradable polymer with a sharp T_m around 60 °C which could be adjusted ranging from 19 to 62 °C by modifying the PCL chain length [3, 4].

Typically, polymerization of ε-caprolactone (CL) is started by ring-opening polymerization (ROP) method. To date, in several investigations on the modification of PCL melting point, it has been observed that by introducing the hydroxyl rich initiators as backbone, available hydroxyl groups are much enough to short the PCL chain length and modulate its T_m. Therefore, a branched architecture was used in PCL system, and relatively short PCL segments were employed as another means of lowering T_m [5]. Liang and co-workers [6]

✉ Massoumeh Bagheri
massoumehbagheri@yahoo.com

✉ Fahimeh Farshi
fahimeh.farshi@g.mail.com

1   Chemistry Department, Science Faculty, Azarbaijan Shahid Madani University, P.O. Box: 537140-161, 5375171379 Tabriz, Iran

2   Polymer Engineering Faculty, Sahand University of Technology, Postal Code: 5331711111, New Town of Sahand, Tabriz, Iran

⧓ Springer

reported three-arm polymers as thermally induced biodegradable polymers based on glycerol and PCL. The star shape design was critical in achieving a T_m near biologically relevant temperatures. Nagahama et al. [7] developed novel biodegradable consisting of star shape branched oligo(ε-caprolactone). Recently, Bai and co-workers [8] demonstrated that introducing of ethyl cellulose as backbone to polymer network can modulate the T_m and mechanical strength of PCL materials.

In this study, we report on the synthesis and characterization of hydroxylpropyl cellulose (HPC) and CL graft copolymers (HPC-g-PCL) with well-defined structure, controlled molecular weight, and desired thermal properties, which were prepared via "grafting from' method using opening polymerization (ROP). HPC is one of the most important nontoxic, biodegradable, and biocompatible cellulose derivatives which is extensively used in producing the smart materials, in biomedicine [9–12]. Structurally, HPC has three hydroxyl groups per each monomeric unit. Therefore, it was selected as initiator due to the adequate number of hydroxyl groups and its bioactive feature [13]. HPC is essential to lowering the crystallinity so that a reduced T_m could be observed for HPC-g-PCL copolymer. The hexamethylene diisocyanate (HDI) was applied to prepare crossinked HPC-g-PCL (X(HPC-g-PCL)) as a biocompatible and biodegradable polymer at body temperature.

Most optimization studies during the development of a novel polymeric system involve variation of one factor at a time, keeping all other factors constant. This traditional optimization method is time-consuming and expensive. Today, a statistical-based technique of response surface methodology (RSM) is used extensively to elucidate the interaction between reaction parameters for optimization. RSM is a technique where by reaction parameters are varied simultaneously in a suitable manner to generate data for development of empirical models. It is a faster and more economical analytical approach than the traditional ones. RSM has been commonly used for designing and optimization of different polymeric systems prepared via ROP, such as grafted PCL to cellulose nanocrystals [14], copolymers of polylactide and polyglycolide (PLGA) as tissue scaffold and drug release device [15], and copolyester involving δ-gluconolactone as a new bio-based product [16]. However, there is not any published information about the optimization of graft polymerization of CL in the presence of HPC and crosslinking reaction of the obtained copolymer.

The current study aims to model and optimize the synthesis of X(HPC-g-PCL) and predicting the T_m in various operating conditions using RSM approach. RSM was used to investigate the effect of reaction parameters (variables) including the monomer content (weight ratio of CL/HPC), catalyst concentration and crosslinker amount on the T_m of X(HPC-g-PCL). Therefore, the novelty of the present study is the use of the RSM approach for optimization of the resultant copolymer X(HPC-g-PCL) in order to get the best option for its use as a new bio-based SMP. Further, we will investigate the shape

memory behaviors of the X(HPC-g-PCL) films with appropriate T_m in continue.

Experimental

Materials

Hydroxypropyl cellulose (HPC) was purchased from Aldrich (Milwaukee, WI, USA; Mn=100,000 gmol^{-1} according to the manufacturer) and dried under vacuum at room temperature for 24 h before use. The molar substitution of propoxy groups (MS$_{HPC}$) was approximated 1.25 using ^{1}H NMR spectrum of HPC [17]. ε-Caprolactone (CL) was purchased from Merck (Germany) and dried over freshly powdered CaH$_2$ for 24 h and then purified by twice distillation under reduced pressure [13]. Tin (II) bis (2-ethylhexanoate) (Sn(Oct)$_2$, 96 %) was purchased from Alfa Acer. Hexamethylene diisocyanate (HDI) was purchased from Fluka and was used without further purification. N, N$^{'}$-Dimethylformamid (DMF) was dried with 4 Å molecular sieves and distilled under reduced pressure before use. Chloroform (CHCl$_3$) and n-hexane were used without further purification.

Synthesis

Synthesis of HPC-g-PCL graft copolymers

A series of HPC-g-PCL graft copolymers having different chain lengths of graft PCL were prepared by ROP of CL in bulk condition. The recipes for preparing the series of HPC-g-PCL (with 85–93 wt.% of CL) are summarized in Table 1. All the polymers were prepared in a similar manner. Therefore, HPC and CL at appropriate weight ratio were charged into a dry flask, mixed thoroughly, and left at room temperature for 12 h until HPC was completely swelled by CL. The mixture was placed in an oil bath at 130 °C under argon atmosphere, then a certain amount of Sn(Oct)$_2$ (Table 1) was dissolved in dry toluene (250 μL) and added immediately into the mixture and was stirred for 24 h at the same temperature. For removing PCL homopolymer as the main by-product during the reaction, it was cooled to room temperature; the resulting polymer was dissolved in THF at a concentration of 5 % (w/v) and then precipitated in equal volume of cold n-hexane. The purification procedure was repeated three times and the pure resultant polymer was dried in vacuum at room temperature to a constant mass.

Preparation of X(HPC-g-PCL) films

The films of X(HPC-g-PCL) were prepared using two different routes.

In route (I), HPC-g-PCL (0.1 g) was dissolved in 4 mL of anhydrous DMF by vigorous stirring until a homogenous solution was obtained. Then enough amount of HDI (Table 2)

Table 1 DSC results for HPC-*g*-PCL copolymers

HPC-*g*-PCL	CL:HPC:Sn(Oct)$_2$ (wt/wt/wt)	T_m (°C)	T_c (°C)	$X_c^{(a)}$ (%)	ΔH_m (J/g)
HPC-*g*-PCL-85 (A)	100:17.65:1.47	47.72	11.24	18.21	−24.58
HPC-*g*-PCL-87 (B)	100:14.90:0.76	48.08	11.12	27.18	−36.70
HPC-*g*-PCL-87 (C)	100:14.90:2.11	51.90	16.13	25.94	−35.02
HPC-*g*-PCL-90 (D)	100:11.11:0.28	56.15	24.24	30.32	−34.40
HPC-*g*-PCL-90 (E)	100:11.11:1.39	50.67	15.50	33.04	−44.61
HPC-*g*-PCL-90 (F)	100:11.11:2.50	51.22	11.27	29.99	−40.49
HPC-*g*-PCL-93 (G)	100:7.56:0.699	52.34	22.55	32.87	−44.37
HPC-*g*-PCL-93 (H)	100:7.56:1.98	54.70	23.34	32.47	−43.83
HPC-*g*-PCL-93 (I)	100:5.26:1.32	56.07	25.15	32.98	−44.52

$^{(a)}$ $X_c = \frac{\Delta H_m}{\Delta H_{100\%}} \times 100$, where the melting enthalpy for 100 % crystalized PCL was considered 135 J/g [8]

was added and before pouring into a Teflon dish, was stirred at 80 °C under argon for about 2 h. After casting the solution, to complete the reaction, the mixture was cured and dried in an oven at 80 °C for 24 h.

In route (II), after dissolving the same amount of HPC-*g*-PCL in 5 mL of anhydrous CHCl$_3$, enough amount of HDI (Table 2) was added to the stirred solution. The mixture was poured into a Teflon dish and left at room temperature for 12 h. For more drying and curing, the casted film was heated in an oven at 80 °C for about 24 h.

Determination of molar substitution (MS$_{CL}$)

Molar substitution of CL (MS$_{CL}$) in HPC-*g*-PCL molecules, which is the average number of CL molecules reacted with each anhydroglucose unit, was determined with a gravimetric method [13]. The calculation is given as follows:

$$MS_{CL} = \left[(W_{graft} - W_{HPC})/114 \right]/(W_{HPC}/234)$$

where W$_{graft}$ is the weight of HPC-*g*-PCL after purification, W$_{HPC}$ is the initial weight of HPC, 114 is the molecular weight of a repeating unit of PCL, and 234 is the average molecular weight of a repeating unit of HPC. In this calculation, HPC was assumed to be 100 % converted to HPC-*g*-PCL Fig. 1.

Etermination of side-chain length and distribution

Various graft lengths of HPC-*g*-PCL copolymers were obtained by adjusting the molar ratios of CL monomer to HPC. The average length of the PCL side chains (*L*) on each HPC repeating unit could be estimated from end-group analysis by ^{1}H NMR spectroscopy. The intensity of the *a* and *e* protons at 2.3 and 4.6 ppm, respectively (see Fig. 2) was used for this purpose. The calculation is given as follows:

$$L = I_{Ha}/(I_{Ha}) - (I_{He})$$

where I_{He} is the peak intensity of the *e* protons that are not at the chain end and I_{Ha} is the peak intensity of the *e* and *e′* protons (peaks overlapped).

The average number of PCL chains on each HPC repeating unit (*N*) was then calculated by

$$N = MS_{CL}/L$$

RSM experimental design and model development for optimized synthesis of HPC-g-PCL

In synthesis process, some parameters such as CL/HPC weight ratio, and catalyst and crosslinker amounts affect the T_m. The influence of operational parameters in the conventional methods has been investigated by systematically varying a parameter and keeping constant the others. This should be repeated for all the influencing parameters, resulting in a large number of experiments. To model the process, using the experimental design methodologies such as RSM can be useful.

The design procedure for RSM is as follows [18]: (i) Performing a series of experiments for adequate and reliable measurement of the response of interest; (ii) developing a mathematical model of the second-order response surface with the best fit; (iii) determining the optimal set of experimental parameters that produce a maximum or minimum value of response; (iv) representing the direct and interactive effects of process parameters through two and three-dimensional (3D) plots. Using RSM, it is possible to estimate linear, interaction and quadratic effects of the factors and a prediction model for the response. In this way, RSM designs could be used to find improved process settings in an efficient use of resources.

In this paper, modeling of the synthesis process was studied using central composite design (CCD) under RSM. In CCD, the response surface is modeled by fitting a second-order polynomial with the number of experiments equal to $2^f + 2f + n_c$, where *f* and n_c are the number

Table 2 DSC results for X(HPC-g-PCL) copolymers

Route I						Route II					
X(HPC-g-PCL)	HDI %W/W	T_m (°C)	T_c (°C)	X_c (%)	ΔH_m (J/g)	X(HPC-g-PCL)	HDI %w/w	T_m (°C)	T_c (°C)	X_c (%)	ΔH_m (J/g)
A'	25.0	42.94	6.72	15.05	−20.32	A''	15.0	32.88	–	–	–
B_1'	16.1	46.58	15.28	20.25	−27.34	B_1''	9.10	37.67	–	0.52	−0.70
B_2'	33.9	44.60	7.58	16.53	−22.34	B_2''	21.9	32.49	–	–	–
C_1'	16.1	48.11	15.24	17.34	−23.41	C_1''	9.10	41.63	2.37	15.69	−21.18
C_2'	33.9	46.62	15.05	12.87	−17.37	C_2''	21.9	38.82	–	0.34	−0.46
D'	25.0	48.26	16.74	14.38	−19.41	D''	15.0	35.76	–	–	–
E_1'	40.0	47.79	21.23	22.29	−30.09	E_1''	25.0	36.32	–	0.79	−1.07
E_2'	25.0	49.73	18.44	22.75	−30.71	E_2''	15.0	38.91	0.69	2.05	−2.77
E_3'	25.0	48.93	17.35	21.58	−29.13	E_3''	15.0	40.11	2.07	2.84	−2.78
E_4'	25.0	48.11	17.56	21.06	−28.43	E''	15.0	38.02	–	1.55	−2.09
E_5'	25.0	50.00	19.01	23.72	−32.02	E_5''	15.0	39.35	1.18	2.93	−3.95
E_6'	25.0	49.05	17.69	21.88	−29.54	E_6''	15.0	37.47	–	–	–
E_7'	25.0	49.34	18.04	22.23	−30.01	E''	15.0	38.55	0.35	1.83	−2.47
E_8'	10.0	50.04	19.32	26.48	−35.64	E_8''	5.00	46.30	15.41	26.34	−35.56
F'	25.0	49.23	15.77	23.15	−35.64	F''	15.0	44.29	8.55	8.65	−11.68
G_1'	16.1	52.74	23.13	24.41	−31.25	G_1''	9.10	40.53	0.55	13.90	−18.77
G_2'	33.9	53.22	20.31	26.91	−32.95	G_2''	21.9	33.32	–	0.11	−0.15
H_1'	16.1	53.22	22.63	24.98	−36.33	H_1''	9.10	43.80	12.71	18.26	−24.85
H_2'	33.9	50.80	15.09	19.57	−33.73	H_2''	21.9	37.64	–	3.09	−4.18
I'	25.0	54.57	25.63	24.78	−26.42	I''	15.0	40.03	3.74	16.71	−22.56

of design factors and center runs, respectively. The CCD consists of three distinct portions: (1st) 2^f fractional points where the factor levels are coded to the usual low and high values (−1, +1); (2nd) $2f$ axial points or "star" points on the axis of each variable at a distance α from the designed center where $\alpha = (2^f)^{1/4}$; and (3rd) n_c center points that can be replicated to provide an estimate of experimental error variance. Therefore, each independent variable was varied at five levels (denoted as coded values $-\alpha$, −1, 0, +1, $+\alpha$) [19]. In this study, α value was fixed at 1.68. The variables studied were HPC/CL ratio (X_1), amount of catalyst (X_2), and amount of crosslinker (X_3). Thus, for synthesis process having three independent parameters, the total number of experiments required was calculated as Eq. (1):

$$N = 2^f + 2f + nc = 2^3 + (2 \times 3) + 6 = 20 \qquad (1)$$

Minitab software was used for both the design and statistical analysis of the experimental data. An analysis of variance (ANOVA) was used to estimate the statistical parameters. The experimental design runs generated by software is shown in Table 3. The setup consist of 20 runs in random order allows modeling of all parameter effects on response.

In Table 3, process factors and their investigated levels are given in coded and actual values. The relationship between the

coded (x) and actual (X) values of the variables is according to Eq. (2):

$$coded\ value = \frac{actule\ value - \frac{(high\ value + low\ value)}{2}}{\frac{(high\ value - low\ value)}{2}} \qquad (2)$$

The outcome of each experimental run is analyzed and the response is correlated with three input factors through an empirical second degree polynomial equation as given by the Eq. (3) [20]:

$$Y = b_0 + \sum_{i=1}^{n} b_i x_i + \sum_{i=1}^{n} b_{ii} x_i^2 + \sum_{i=1}^{n} \sum_{j=1}^{n-1} b_{ij} x_i x_j \qquad (3)$$

where, Y is the predicted response (T_m, °C), b_0 the constant coefficient, b_i the linear coefficients, b_{ij} the interaction coefficients and b_{ii} the quadratic coefficients of the factors.

Instrumental

FT-IR spectra were recorded on a Brucker PS-15 spectrometer (Bruker Optics, Ettlingen, Germany) at wave numbers ranging from 400 to 4000 cm^{-1}. ^{1}H NMR spectra were taken on a 400 MHz Brucker SP-400 Avance spectrometer (Bruker Biospin, Rheinstetten, Germany) using chloroform as solvent

Fig. 1 FT-IR spectra of **a** HPC, **b** HPC-*g*-PCL, and **c** X(HPC-*g*-PCL)
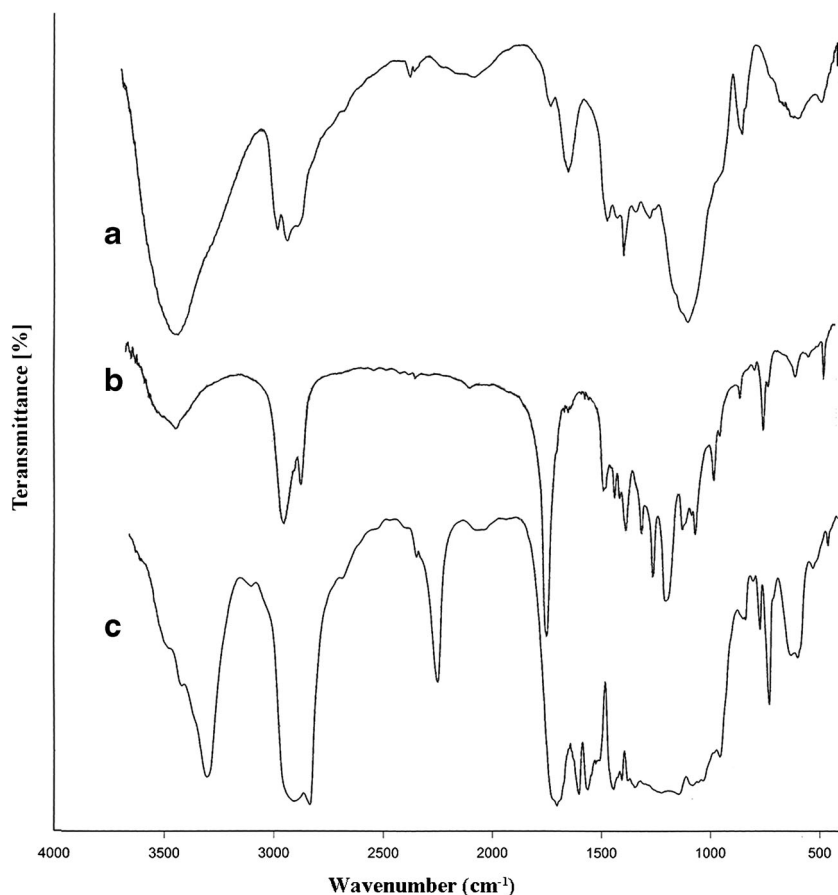

with tetramethylsilane as the internal standard. A Mettler-Toledo model 822 differential scanning calorimeter (Columbus, OH, USA) was used to determine phase transition temperatures at heating and cooling rates of 10 °C/min. The instrument was calibrated with indium regarding temperature and enthalpy. Enthalpy change (ΔHm), melting temperature (Tm) and crystallinity (Xc) were obtained from the second heating curves. The crystalline structure of the products were analyzed using X-ray diffraction (XRD) patterns by a Bruker AXS model D8 advanced diffractometer for Cu Kαradiation ($\lambda=1.54187$ Å) at 40 kV and 35 mA with Bragg angle ranging from 3 to 70°.

Results and discussion

Synthesis and structural analysis of HPC and PCL based copolymers

The synthetic routes for the HPC-*g*-PCL and its crosslinked copolymers are shown in Schemes 1. In this study, the graft copolymerization of CL was initiated by a hydroxyl-group-rich HPC in the presence of Sn(Oct)$_2$ catalyst in a bulk condition. ROP method was chosen since it is well-known for CL to form either a homopolymer or copolymers [13]. Therefore, a series of HPC-*g*-PCL copolymer with different CL/HPC ratios and catalyst amounts were prepared and named as HPC-*g*-PCL-N (N is related to the weight percent of CL in HPC-*g*-PCL synthesis). Then the corresponding X(HPC-*g*-PCL) were obtained by crosslinking with different amounts of HDI through two different routes (route I and route II). We
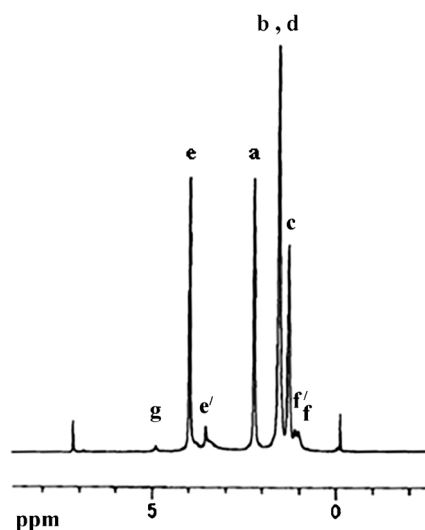
Fig. 2 ^{1}H NMR spectrum of HPC-*g*-PCL

Table 3 Experimental design matrix and response matrix for route I and route II

Run	Coded value			Actual value						$T_m{}^*$ (°C)	
	x_1	x_2	x_3	Route I			Route II				
				X_1	X_2	X_3	X_1	X_2	X_3	Route I	Route II
1	0.00	0.00	0.00	90.00	1.25	25.00	90.00	1.25	15.00	49.73	38.91
2	0.00	0.00	+1.68	90.00	1.25	40.00	90.00	1.25	25.00	47.79	36.32
3	0.00	0.00	0.00	90.00	1.25	25.00	90.00	1.25	15.00	48.94	40.11
4	−1.00	−1.00	−1.00	87.03	0.66	16.08	87.03	0.66	9.05	45.58	37.67
5	0.00	0.00	−1.68	90.00	1.25	10.00	90.00	1.25	5.00	50.04	46.30
6	0.00	0.00	0.00	90.00	1.25	25.00	90.00	1.25	15.00	48.11	38.02
7	+1.00	+1.00	−1.00	92.97	1.84	16.08	92.97	1.84	9.05	53.22	43.80
8	−1.00	+1.00	−1.00	87.03	1.84	16.08	87.03	1.84	9.05	48.11	41.63
9	−1.00	+1.00	+1.00	87.03	1.84	33.92	87.03	1.84	20.95	46.62	38.32
10	−1.00	−1.00	+1.00	87.03	0.66	33.92	87.03	0.66	20.95	44.60	32.49
11	+1.68	0.00	0.00	95.00	1.25	25.00	95.00	1.25	15.00	54.57	40.03
12	0.00	0.00	0.00	90.00	1.25	25.00	90.00	1.25	15.00	50.00	39.35
13	0.00	0.00	0.00	90.00	1.25	25.00	90.00	1.25	15.00	49.05	37.47
14	0.00	0.00	0.00	90.00	1.25	25.00	90.00	1.25	15.00	49.34	38.55
15	+1.00	+1.00	+1.00	92.97	1.84	33.92	92.97	1.84	20.95	50.80	37.64
16	0.00	+1.68	0.00	90.00	2.25	25.00	90.00	2.25	15.00	49.23	44.29
17	+1.00	−1.00	+1.00	92.97	0.66	33.92	92.97	0.66	20.95	53.22	33.32
18	0.00	−1.68	0.00	90.00	0.25	25.00	90.00	0.25	15.00	48.26	35.76
19	−1.68	0.00	0.00	85.00	1.25	25.00	85.00	1.25	15.00	42.94	32.88
20	+1.00	−1.00	−1.00	92.97	0.66	16.08	92.97	0.66	9.05	52.74	40.53

* Each run was repeated 3 times and the average value was taken to ensure the results
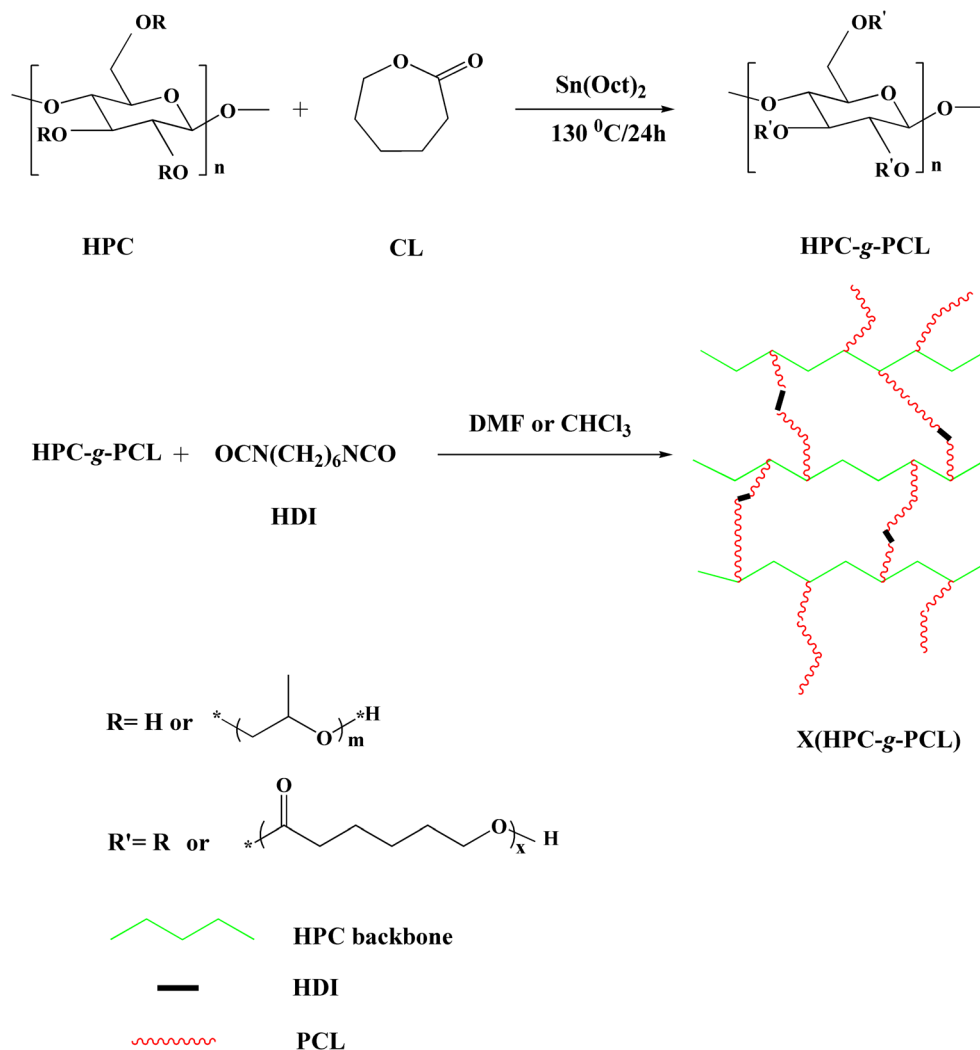
first attempted to synthesize X(HPC-g-PCL) by reacting terminal hydroxyl functional groups of PCL grafts with HDI in DMF at 80 °C for 2 h, as shown in Scheme 1, route I. However, the mild condition for the synthetic approach (Scheme 1, route II) was the second route to crosslink the HPC-g-PCL with the same crosslinker in the chloroform at room temperature for 12 h.

The structures of HPC-g-PCL and the crosslinked product were characterized with FT-IR and ^{1}H NMR spectroscopies. The FT-IR spectra of HPC, HPC-g-PCL and X(HPC-g-PCL) are depicted in Fig. 1. As shown in HPC-g-PCL spectrum (Fig. 1b), in comparison with the HPC spectrum (Fig. 1a), a new peak appearing at 1732 cm^{-1} can be attributed to the C=O stretching of the PCL segment in HPC-g-PCL [21]. In Fig. 1c, a clear evidence for cross-linking the copolymer resulted from the stronger and wider absorption peak of C=O in cross-linked film in comparison with HPC-g-PCL due to the presence of carbamate and ester peaks. The spectrum of crosslinked HPC-g-PCL shows a new sharp absorption band at 3329 cm^{-1}, which was ascribed to the N-H stretching vibration of the urethane bonds [7, 8]. Another variation associated with the crosslinks in the copolymer is an enhancement in the intensity of C-H stretching resonances from the methylene groups which resonate at 2926 and 2854 cm^{-1} (Fig. 1c). These results confirmed that the grafting of PCL onto HPC and subsequent crosslinking through terminal hydroxyl groups of PCL grafts by HDI was performed successfully [22, 23].

The ^{1}H NMR spectra of HPC-g-PCL are displayed in Fig. 2. The spectra were recorded in CDCl$_3$ at 25 °C. The signals at 2.12 and 1.21 ppm (f, f') arise through the splitting of the signal due to methyl protons in the hydroxypropyl groups by the ester groups formed during the graft reaction. It is apparent that besides the dominant HPC signals, there is new very small peak (g) at 5.0 ppm in HPC-g-PCL spectrum which was assigned to the methine protons in the hydroxypropyl groups bonded directly to the PCL chains [13]. Due to the low content of HPC in the copolymers, the HPC signals were not observed in spectrum.

On the basis of the gravimetric method and assignment and integration of the ^{1}H NMR spectrum of HPC-g-PCL, the average number of CL molecules reacted with each anhydroglucose unit (MS$_{CL}$), the average length of the PCL side chains (L) and the number of the side chains on each HPC repeating unit (N) could be estimated (see Experimental section). The results of MS$_{CL}$ for copolymers HPC-g-PCL-85

Scheme 1 Synthetic route of HPC-g-PCL and X(HPC-g-PCL)

HPC   **CL**   **HPC-g-PCL**

HPC-*g*-PCL + OCN(CH$_2$)$_6$NCO

HDI

DMF or CHCl$_3$

X(HPC-*g*-PCL)

R= H or

R'= R or

HPC backbone

HDI

PCL

and HPC-*g*-PCL-95 (with lowest and highest amount of CL/ HPC) are 4.8 and 26.6, respectively. The errors were considered from MS$_{CL}$ estimation with the ^{1}H NMR spectroscopy method as reported earlier [13]. The L and N values for synthesized HPC-*g*-PCL copolymers varied from 20.2 to 24.0 and 0.2 to 1.1, respectively, with increasing of CL content (85 to 95 %). Hence, on average, for HPC-*g*-PCL-85 and HPC-*g*-PCL-95, there were 2 and 11 PCL side chains attached to 10 HPC repeating units with length of 20 and 24, respectively.

Thermal analysis

The thermal properties of HPC-*g*-PCL and X(HPC-*g*-PCL) copolymers were characterized using DSC. The curves from the second heating run are shown in Fig. 3. Their main thermal characteristic are summarized on Tables 1 and 2, in terms of melting and crystallization temperature, T_m and T_c, respectively, as well as melting enthalpy, ΔH_m. HPC is an amorphous polymer without any sharp melting peak. However, as shown in Table 1, HPC-*g*-PCL, depending on the CL/HPC ratio (85–

93 %) exhibits a sharp melting peak ranging from 47.7 to 56.1 °C. The T_m and X_c of HPC-*g*-PCL increased with increasing PCL content [8] which could be easily concluded from Table 1 and Fig. 3a and b. Generally, T_m of HPC-*g*-PCL is lower than that of PCL due to the decreased crystallinity of PCL grafts which in turn has resulted from the inhibited crystal formation via the incorporation of amorphous HPC backbone. In a way that the resulted HPC-*g*-PCL which contains well shortened side chains (graft copolymer synthesized without using the catalyst) did not show any T_m from DSC thermogram.

As seen in Table 1, T_m is also dependent on the content of Sn(Oct)$_2$ catalyst on the ROP of CL. Using the same CL/HPC ratio (i.e., samples D and E; Table 1), decreased in T_m, and in the corresponding ΔH_m and X_c values, were observed for HPC-*g*-PCL by using higher amount of catalyst ($T_m=$ 56.1 °C and 50.7 °C for D and E, respectively). Indeed, enhancement of the initial concentration of catalyst essentially increased the overall number of active chain ends in the melt, resulting in lower length of side chain. The contrary, using higher amount of catalyst (i. e. sample F; Table 1) increasing

Fig. 3 DSC curves of recorded on the second heating run of **a** HPC-*g*-PCL-93 (G), **b** HPC-*g*-PCL-87 (B), **c** X(HPC-*g*-PCL-93) (G$_1'$), **d** X(HPC-*g*-PCL-87) (B$_1'$), and **e** X(HPC-*g*-PCL-93) (G$_1''$), and **f** X(HPC-*g*-PCL-87) (B$_1''$)
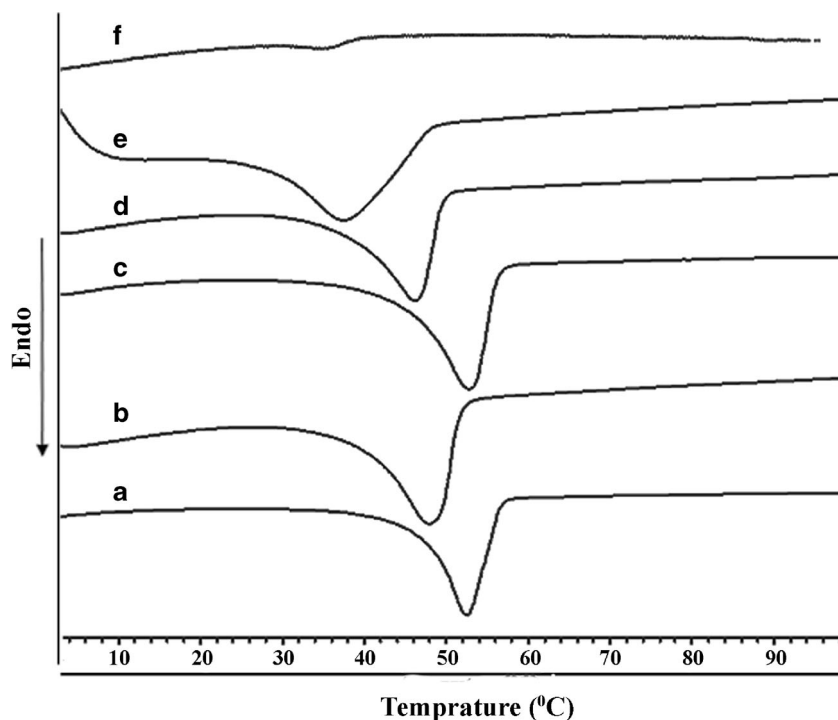

the T_m was observed. This dependence can be explained obviously based on activation of all hydroxyl groups on the HPC, resulting in higher rates of monomer consumption [24].

In our study, X(HPC-*g*-PCL) by using different amount of HDI and HPC-*g*-PCL was synthesized through two crosslinking routes. As shown in Fig. 3c to f, melting is observed for X(HPC-*g*-PCL), confirming the presence of crystalline phases in the films. The crosslinked films also showed a decreased ΔH_m and X_c compared to those of the corresponding HPC-*g*-PCL due to the decreased quantity of crystalline phase in X(HPC-*g*-PCL) (Table 2).

As listed in Table 2, notable decrease in T_m are observed upon network formation indicating that network formation had a strong influence on the degree of crystallinity via more limitation in movement of PCL chains [7, 8, 25]. The melting temperature of X(HPC-g-PCL-85) decreased with increasing of HDI content and it declined to 42.9 °C and 32.9 °C at 25.0 and 15.0 % of HDI via route I and route II, respectively (A$'$ and A$''$, Table 2). As the resulted X(HPC-g-PCL) (containing 85–95 % CL) via route II by using higher than 22 % HDI did not show any T_m from DSC thermogram (Table 2). When the crosslinking route II was used, both X_c and T_m dropped largely, which might result from the mild reaction conditions of route II and increasing of crosslinking efficiency.

The variation of crystallinity can also be confirmed by XRD analysis. As shown in Fig. 4a and b, spectra of HPC-*g*-PCL with different PCL contents displays well defined crystalline diffraction peaks at $2\theta = 21.56$ and 23.84°, in agreement with those reported for PCL in the literature [26], with increased of crystalline diffraction with the former due to its

greater MS$_{CL}$. These results suggest that the partially crystalline phase in the HPC-*g*-PCL originated from the PCL side chains. On the other hand, there were significant crystallinity
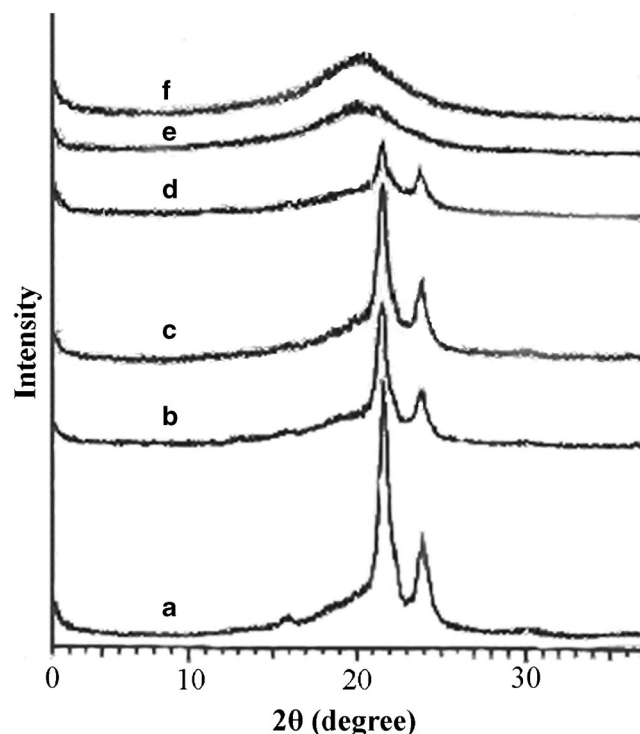
Fig. 4 Wide-angle X-ray diffraction patterns of **a** HPC-*g*-PCL-93 (G), **b** HPC-*g*-PCL-87 (B), **c** X(HPC-*g*-PCL-93) (G$_1'$), **d** X(HPC-*g*-PCL-87) (B$_1'$), and **e** X(HPC-*g*-PCL-93) (G$_1''$), and X(HPC-*g*-PCL-87) (B$_1''$) recorded at 25 °C

differences in crosslinked films (Fig. 6c to f). Similar to the results obtained from DSC analysis, the intensity of crystalline diffraction peaks of PCL also decreased in crosslinked films, especially for prepared film via route II, while it increased at $2\theta=20.24°$ (Fig. 4e and f). According to the DSC and XRD results, the crystallininty of these grafted copolymers and crosslinked films were mostly changed from a semicrystalline to an amorphous material depending on the amount of grafting PCL and degree of crosslinking.

RSM results

Model design and statistical analysis

To obtain the polynomial model representing the T_m (response) as a function of HPC/CL weight ratio, catalyst, and crosslinker amounts (factors), the data for two routes, shown in Table 3, were used. The data were analyzed using Minitab software to provide analysis of variance (ANOVA), regression coefficients, and regression. A regression equation for different factors was obtained after ANOVA. All terms regardless of their significance are included in the following fitted second-order polynomial equations in terms of the coded variables for route I (Eq. 4) and route II (Eq. 5):

$$q = 49.1763 + 3.2679x_1 + 0.3106x_2 - 0.6000x_3 - 0.0332x_1^2 - 0.0367x_2^2 + 0.0234x_3^2 - 0.8112x_1x_2 + 0.0662x_1x_3 - 0.4263x_2x_3 \tag{4}$$

$$q = 38.7692 + 1.2232x_1 + 2.3597x_2 - 2.7931x_3 - 1.0293x_1^2 + 0.2328x_2^2 + 0.6872x_3^2 - 0.3375x_1x_2 - 0.6725x_1x_3 + 0.4275x_2x_3 \tag{5}$$

The adequacy of the regression models for explaining the experimental data at a 95 % confidence level was tested by analysis of variance (ANOVA) results. The ANOVA includes some statistic factors such as lack of fit, R^2, and adjusted R^2. From ANOVA results (Table 4) it is found that the fit of models for two routes were very satisfactory, as P-values for both

routes were 0.000 (P-value<0.05). Also, the coefficients of determination (R^2) and adjusted coefficients of determination (R_{Adj}^2) were 97.3, 94.9 % for route I and 93.3, 87.4 % for route II. These indicated only 2.7 % in route I and 6.7 % in route II of the total variability were not explained by the repressors in the models. The high R^2 value indicated that the obtained model gives a good estimate of response of the system in the studied range. Joglekar and May suggested that for a good fit of a model, R^2 should be at least 80 % [27]. The insignificance "lack of fit" with P-values of 0.506 for route I and 0.145 for route II (P-value>0.05) indicated that the models satisfactorily fitted the data. A comparison between calculated and experimental values of the T_m in two routes by using the resulted second-order polynomial Eqs. (4) and (5) were shown in Fig. 5. These plots confirm that the experimental values are in good agreement with the predicted values.

All terms in the regression model are not equally important. The significance of each term was determined by student's T-test and P-values data (Table 5). The T-values represent the ratio of the estimated parameter effect to the estimated parameter standard deviation. The larger the magnitude of the T-value and smaller the P-value of the coefficients represent the more significance [28]. In route I results of the T-value and P-value imply that the linear effects of monomer content (ratio of CL/HPC) and crosslinker amount are more significant. Also the interactive effect of monomer-crosslinker is important whereas catalyst amount, square effect of monomer, square effect of catalyst, square effect of crosslinker, interactive effect of monomer-crosslinker and interactive effect of catalyst-crosslinker have no significant influence on the T_m. In route II the results indicate that the linear effects of monomer, catalyst, and crosslinker are more significant. Also the square effect of monomer is important whereas square effect of catalyst, square effect of crosslinker, interactive effect of monomer-catalyst, interactive effect of monomer-crosslinker and interactive effect of catalyst-crosslinker have no significant influence on the T_m.

Table 4 Analysis of variance for route I and route II

Source	Degree of freedom		Sum of squares		Mean square		F-value		P-value	
	M 1	M 2	M 1	M 2	M 1	M 2	M 1	M 2	M 1	M 2
Regression	9	9	158.876	234.365	17.6529	26.0405	40.08	15.60	0.000	0.000
Linear	3	3	152.078	203.014	50.6925	67.6714	115.08	40.53	0.000	0.000
Square	3	3	0.045	25.359	0.0150	8.4531	0.03	5.06	0.991	0.022
Interaction	3	3	6.754	5.991	2.2512	1.9971	5.11	1.20	0.021	0.360
Residual error	10	10	4.405	16.696	0.4405	1.6696				
Lack of fit	5	5	2.186	12.251	0.4373	2.4501	0.99	2.76	0.506	0.145
Pure error	5	5	2.219	4.445	0.4437	0.8890				
Total	19	19	163.281	251.060						
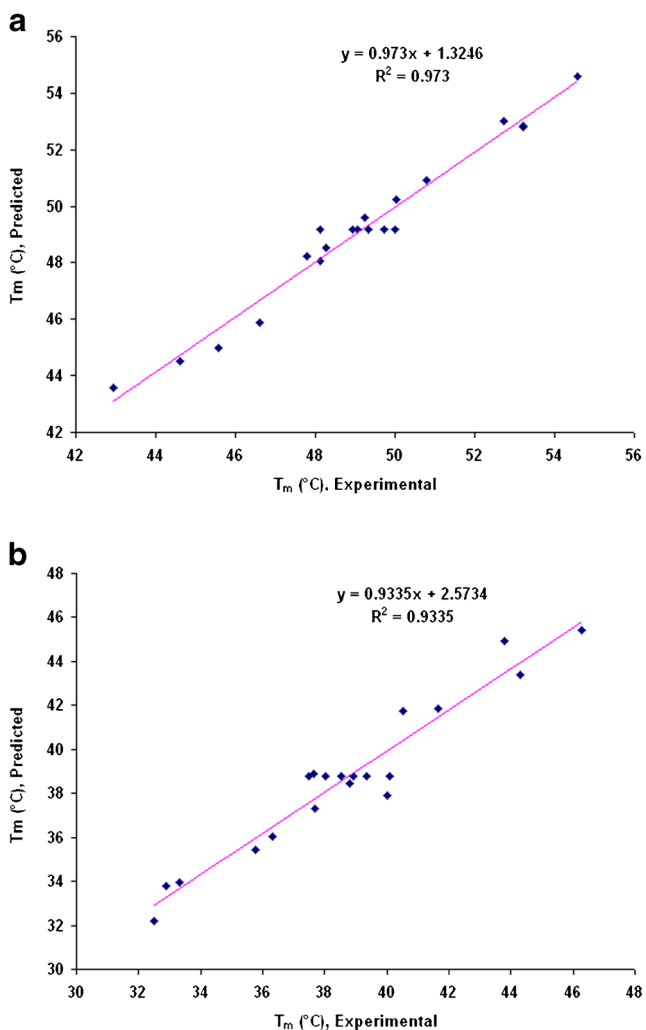
Fig. 5 Plot of predicted results of T_m versus experimental values **a** route I and **b** route II

Fig. 6 Pareto graph for T_m **a** route I and **b** route II

The probability value less than 0.05 calls for the rejection of the null hypothesis indicating that the particular term significantly affects the measured response of the system. The insignificant terms with P-values higher than 0.05 were removed from final expressions of the two models. The final predictive models in terms of the coded variables are presented for route I (Eq. 6) and route II (Eq. 7):

$$q = 49.1763 + 3.2679x_1 - 0.6000x_3 - 0.8112x_1x_2 \qquad (6)$$

Table 5 Estimated regression coefficients and corresponding T-values and P-values from the data of central composite design experiments for method 1 (M 1) and method 2 (M 2)
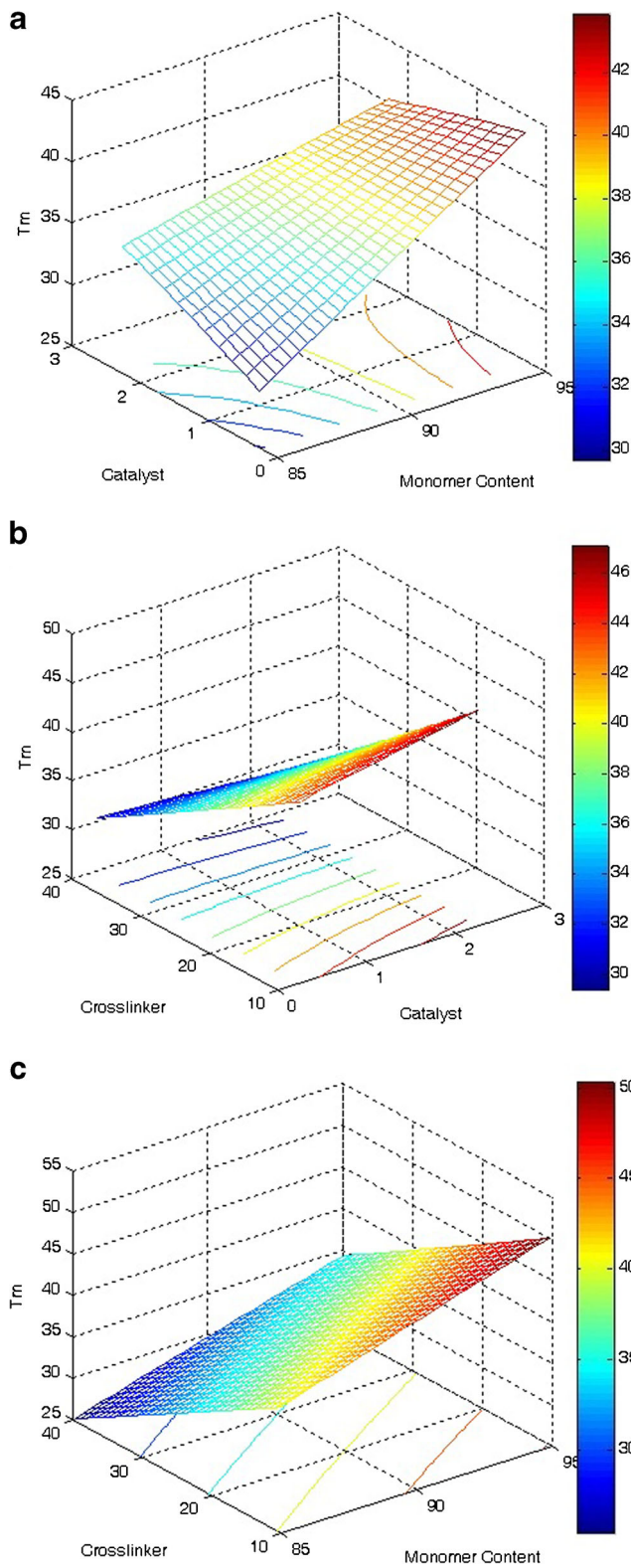
Coefficient	Parameter estimated		Standard error		T-value		P-value	
	M 1	M 2	M 1	M 2	M 1	M 2	M 1	M 2
b_0	49.1763	38.7692	0.2707	0.5270	181.674	73.567	0.000	0.000
b_1	3.2679	1.2232	0.1796	0.3496	18.196	3.498	0.000	0.006
b_2	0.3106	2.3597	0.1796	0.3496	1.729	6.749	0.114	0.000
b_3	−0.6000	−2.7931	0.1796	0.3496	−3.341	−7.988	0.007	0.000
b_{11}	−0.0322	−1.0293	0.1748	0.3404	−0.190	−3.024	0.853	0.013
b_{22}	−0.0367	0.2328	0.1748	0.3404	−0.210	0.684	0.838	0.509
b_{33}	0.0234	0.6872	0.1748	0.3404	0.134	2.019	0.896	0.071
b_{12}	−0.8112	−0.3375	0.2346	0.4568	−3.457	−0.739	0.006	0.477
b_{13}	0.0662	−0.6725	0.2346	0.4568	0.282	−1.472	0.783	0.172
b_{23}	−0.4263	0.4275	0.2346	0.4568	−1.817	0.936	0.099	0.371

Fig. 7 Response surface and contour plots of T_m (route I)

$$q = 38.7692 + 1.2232x_1 + 2.3597x_2 - 2.7931x_3 - 1.0293x_1^2 \quad (7)$$

The pareto analysis is used primarily to identify those factors that have the greatest cumulative effect on the
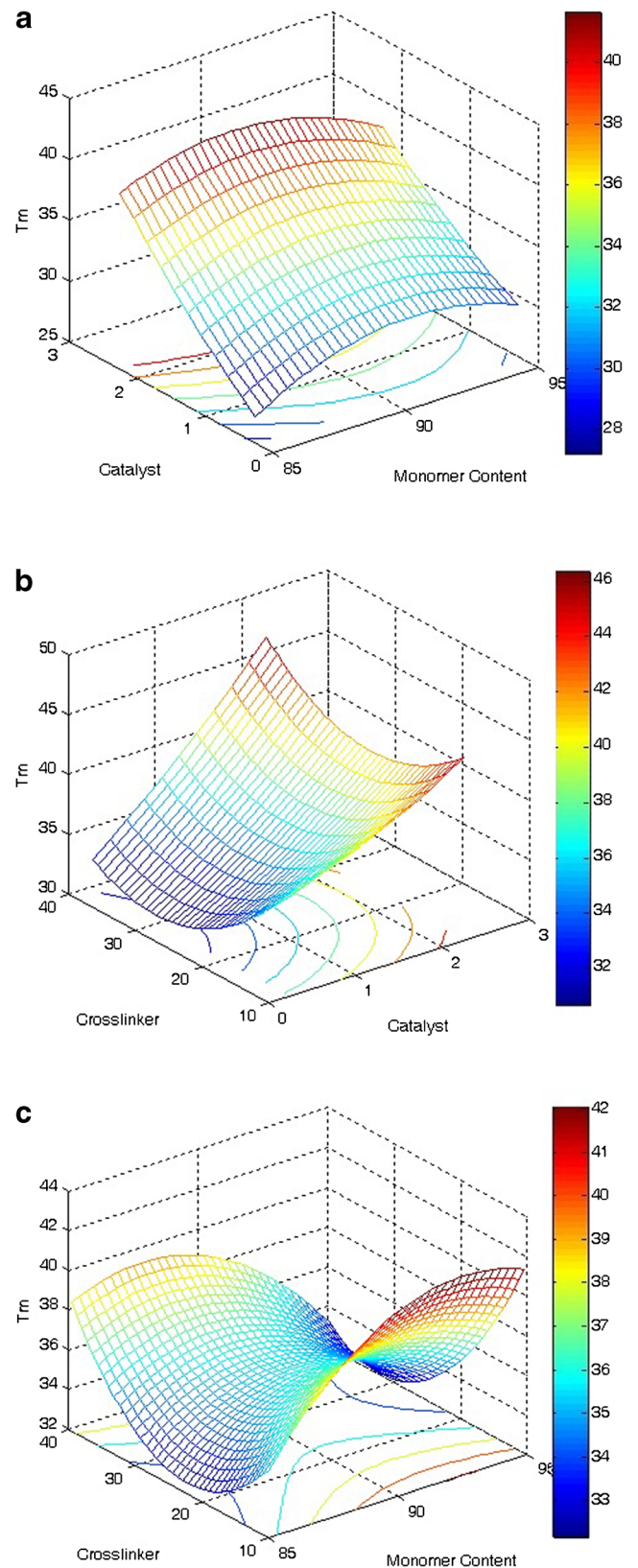
Fig. 8 Response surface and contour plots of T_m (route II)

system, and has screen out the less significant factors. In fact, this analysis calculates the percentage effect of

each factor on the response, according to the Eq. (8) [19]:

$$Pi = \left(\frac{bi^2}{\sum bi^2}\right) \times 100 \ (i \neq 0) \qquad (8)$$

The results presented in Fig. 6 indicated that the important factors are different in two routes. In route I, monomer content and interactive effect of monomer-catalyst were more important. But in route II, monomer content, catalyst amount, crosslinker amount and square effect of monomer content had more influence on T_m.

Response surface and contour plots

The graphical explanation of the factors effects in obtained models are shown using 3D (response surface) and 2D (contour) plots. These plots predict responses by holding one factor at fixed level (normally at the zero level) and the others varying within the experimental ranges using the Minitab software. Response surface plots are helpful to predict the response for different levels of tested factors. Contour plots that give a geometric representation of the underlying response function are useful in understanding both the main and the interaction effects of factors. A circular contour of response surface indicates that the interaction between the corresponding factors is negligible. In contrast, an elliptical or saddle nature of the contour plots indicates that the interaction between the corresponding factors is significant [19].

In the present study the plots of two routes and the determined relationships between the process factors and T_m have shown in Fig. 7(a to c) and Fig. 8(a to c). In accordance with the DSC and XRD results, the RSM results showed that the T_m increased with increasing the ratio of CL/HPC. Also, T_m decreased with increase of crosslinker amount. Furthermore, from results, it can be concluded that the T_m increased with increasing the catalyst amount.

Optimization and verification

The optimum values of selected factors for model were obtained by solving the regression equations. In this work, the value of temperature was the most important constraint because of the biomedical application of the synthesized X(HPC-g-PCL) copolymer. The target value for T_m was selected as 38 °C. The condition for closer value to target temperature in route I was obtained with these factor values: monomer content=85.00, catalyst=0.25and crosslinker= 10.00. The optimum condition for T_m with target value of 38 °C in route II were found to be as follow: monomer content=85.32, catalyst=0.92 and crosslinker=5.00. Under these conditions, the values of T_m in route I and route II predicted by using the optimum values of the factors and model equations were 36.15 °C and 37.70 °C, respectively. A verification of the predicted results was accomplished by performing experiments using the set of optimized factors. The values of T_m in optimum conditions obtained through the experiments were 36.50 °C and 37.65 °C. Therefore, the experimental results were in close agreement with the model predictions. Meanwhile, it was further confirmed that the optimized conditions described in this study would be helpful for the application of synthesized X(HPC-g-CL) copolymer in biomedical applications.

Conclusion

Well-defined HPC-g-PCL copolymers were synthesized by grafting PCL from HPC via ring opening polymerization of CL in the presence of HPC as an initiator and a catalytic amount of $Sn(Oct)_2$. The graft copolymers were crosslinked by HDI under two different routes to prepare chemically crosslinked polymeric network (X(HPC-g-PCL)). Response surface methodology (RSM) was successfully used to optimize the process by using a factorial design approach on three experimental parameters: monomer content, amount of catalyst and crosslinker. In accordance with the DSC and XRD results, the RSM results showed that the T_m increased with increasing the ratio of CL/HPC and catalyst amount and with decreasing the crosslinker amount. Based on the fitted models, the optimum content for the biomedical application of crosslinked HPC-g-PCL films is over 85 wt.% monomer, below 1 wt.% catalyst and 10 wt.% crosslinker. The target value for T_m was selected as 38 °C. These results should be relevant and important for the developments of a novel biodegradable shape-memory materials.

References

1. Ma L, Kang H, Liu R, Huang Y (2010) Langmuir 26:18519–18525
2. Ping P, Wang W, Chen X, Jing X (2005) Biomacromolecules 6: 587–592
3. Zhang D, Giese ML, Prukop SL, Runlan MA (2011) J Polym Sci A Polym Chem 49:754–761
4. Santhosh-Kumar KS, Reghunadhan-Nair CP (2014) RSC Adv 4: 2969–2973
5. Liang C, Rogers CA, Malafeew E (1997) J Intell Mater Syst Struct 8:380–386
6. Xue L, Dai S, Li Z (2009) Macromolecules 42:964–972
7. Nagahama K, Ueda Y, Ouchi T, Ohya Y (2009) Biomacromolecules 10:1789–1794
8. Bai Y, Jiang C, Wang Q, Wang T (2013) Carbohydr Polym 25:522–527
9. Leng J, Lan X, Liu Y, Dua S (2011) Prog Mater Sci 56:1077–1135

10. Ebara M, Uto K, Idota N, Hoffman JM, Aoyagi T (2012) Adv Mater 24:273–278
11. Schuh C, Schuh K, Lechmann MC, Garnier L, Kraft A (2010) Polymers 2:78–85
12. Bagheri M, Shateri S, Niknejad H, Entezami AA (2014) J Polym Res 21:567–582
13. Shi R, Burt HM (2003) J Appl Polym Sci 89:718–727
14. Cabezas LI, Mazarro R, Gracia I, De-Lucas A, Rodríguez JF (2013) Express Polym Lett 7:886–894
15. Tian C, Fu S, Chen J, Meng Q, Lucia LA (2014) Nord Pulp Paper Res 29:58–68
16. Todea A, Biro E, Badea V, Paul C, Cimporescu A, Nagy L (2014) Pure Appl Chem 86:1781–1792
17. Bagheri M, Shateri S (2012) J Polym Res 19:9842–9855
18. Gunaraj V, Murugan N (1999) J Mater Process Technol 88:266–275
19. Miller JN, Miller JC (2005) Statistics and chemometrics for analytical chemistry. Pearson Education, Canada
20. Mirmohseni A, Dorraji SM, Figoli A, Tasselli F (2012) Bioresour Technol 121:212–220
21. Wang C, Dong Y, Tan H (2003) J Polym Sci A Polym Chem 41:273–280
22. Ostmark E, Harrisson S, Wooley KL, Malmstrom E (2007) Biomacromolecules 8:1138–1148
23. Araki J, Kataoka T, Ito K (2008) Soft Matter 4:245–249
24. Storey RF, Sherman JW (2002) Macromolecules 35:1504
25. Liu C, Chun SB, Mather PT (2002) Macromolecules 35:9868–9874
26. Kumar S, Bose S, Chatterjee K (2014) RSC Adv 4:19086–19098
27. Joglekar AM, May AT (1987) Cereal Foods World 32:857–868
28. Rastegar M, Shadbad KR, Khataee AR, Pourrajab R (2012) Environ Technol 33:995–1003